ELSEVIER

Journal of Crystal Growth 158 (1996) 144–152

JOURNAL OF CRYSTAL GROWTH

Interface curvature and convection related macrosegregation in the vertical Bridgman configuration

S. Kaddeche [a,*], J.P. Garandet [b], C. Barat [b], H. Ben Hadid [a], D. Henry [a]

[a] *Ecole Centrale de Lyon / Université Claude Bernard-Lyon 1, Laboratoire de Mécanique des Fluides et d'Acoustique, URA CNRS 263, ECL, BP 163, F-69131 Ecully Cedex, France*

[b] *DTA / CEREM / DEM / SES, Commissariat à l'Energie Atomique, F-38054 Grenoble Cedex 9, France*

Received 2 February 1995; accepted 15 June 1995

Abstract

The interference between natural convection and macrosegregation is investigated numerically over a wide range of relevant parameters for the vertical Bridgman growth configuration. Our code is validated with respect to analytical, numerical and experimental data. In parallel, we propose scaling laws controlling segregation for the different convective regimes that allow for a discussion of the physical mechanisms governing mass transport in the melt. This work is of interest for the practician since an estimation of both radial and longitudinal segregation can be given from the obtained scaling laws.

1. Introduction

It is generally accepted that the control of chemical concentration variations in single crystals grown from the melt is not an easy task. This problem has been thoroughly studied in the past 40 years since an homogeneous composition is a key requirement for most applications. Even though some significant progress has been achieved, a perfect understanding of the segregation phenomena still eludes us; as consequence, a dose of empiricism is still necessary, but it is the purpose of this paper to show that modelling can also be a valuable asset for the practician.

The segregation problem is in principle tractable, since the equations governing mass transfer in the liquid phase were discovered more than a century ago. It is well known that solute transport proceeds by both diffusion (mostly via concentration gradients) and convection. In practice however, the coupling between heat, mass and momentum problems is often extremely complex, specially in multi-dimensional and time dependent systems.

The vertical Bridgman growth configuration appears very interesting for the production of both semiconductor and oxide crystals (see for instance Refs. [1,2]). In the classical three zone configuration, the heat flux generated on the hot side passes through an insulating region and is extracted on the cold end. In gradient furnaces in contrast, the thermal design ensures a constant temperature gradient in both the melt and the crystal.

In practice, the energy flux can never be perfectly one dimensional, due to unavoidable heat exchange between the sample and the crucible. The fluid motion resulting from the radial temperature gradients, even though it is weak in comparison with other

* Corresponding author.

SSDI 0022-0248(95)00316-9

growth techniques, can still significantly influence both axial and radial segregation in vertical Bridgman solidification. On the other hand, since convection in the melt is generally steady, microscale heterogeneity is not a major problem. However, in chemically destabilizing systems such as PbSnTe [3], unsteady Rayleigh–Benard type convection may take place and lead to solute striations.

The numerical modelling of segregation phenomena in the vertical Bridgman configuration has been carried out by Brown and his coworkers in many interesting papers (see for instance Refs. [4–7] and references herein). A pseudo steady state model applied to dilute alloys was used at first [4], but the effect of solutal convection in mixed systems was also considered [5]. State of the art simulations now include transient analysis [6] and coupling with the phase diagram [7].

The computations indicate that for "typical" growth conditions, convection indeed affects solute repartition in the melt. A key result is that radial segregation passes through a maximum at the transition between the diffusive and the convective mass transport regimes. A similar finding was obtained by Motakef [8], who also presents scaling laws governing the interference of fluid flow with solute transport in dilute alloys.

The solute problem in the presence of a non-planar interface was solved analytically by Coriell and coworkers [9,10], assuming purely diffusive conditions. Curvature related segregation is seen to be proportional to interface deflection when the growth velocity is very low [9], and to vanish at both very low and very large growth rates [10]. Their analysis was recently refined by Korpela et al. [11] to allow for interface shapes that match the crucible at arbitrary angles.

In this paper, we take a fresh look at the problem of solute segregation during solidification of dilute alloys in vertical gradient furnace. With respect to previous works in the field, our purpose is not so much the accurate modelling of a given growth experiment, but rather the understanding of the convecto-diffusive processes in the melt. To do so, we shall rely on the association of order of magnitude and scaling analyses, since such an approach proved very successful in previous works [12,13].

For instance, it is well known that the convecto-diffusive parameter Δ that measures the thickness of the solutal boundary layer in the vicinity of the growth interface is a key parameter in the modelling of axial segregation. As in the horizontal Bridgman configuration [12–14], we shall see that this parameter – or equivalently the effective partition ratio – can again be easily estimated knowing the main characteristics of the flow in the vicinity of the interface.

As such, it can be used in a variety of cases, in the fields of axial [12], radial [15,16] and micro [17] segregation. In the frame of our present work, scaling laws for the radial segregation in vertical Bridgman will be identified and compared with the existing literature data. Since our focus is only on dilute alloys, we shall not consider the microsegregation problem in this paper. With respect to Motakef's work [8], we perform a complete modelling of the developed convective regime.

In Section 2, we shall briefly present the mathematical model used for the numerical simulations; Section 3 is dedicated to a validation of our code, against analytical [9], numerical [8] and experimental [18] data. The results on axial and radial segregation will be detailed in Sections 4 and 5, respectively. Finally, our conclusions in terms of experiments design will be discussed in Section 6.

2. Mathematical model

2.1. Governing equations

We consider a cylindrical finite cavity of radius R and height H (see Fig. 1; $A = H/R$ is the initial aspect ratio), filled with a low Prandtl number Newtonian fluid with constant physical properties except for the density which obeys the classical Boussinesq law: $\rho = \rho_0 [1 - \beta(T - T_0)]$, where β is the thermal expansion coefficient. We also assume that the solid–liquid interface moves at a constant velocity V_f and has a parabolic shape. The segregation coefficient k is constant and equal to its equilibrium value. Thus, along the solid–liquid interface, we have the following relationship between the concentration in the liquid C_l and the concentration in the solid C_s: $C_s = kC_l$.

The governing equations (conservation equations

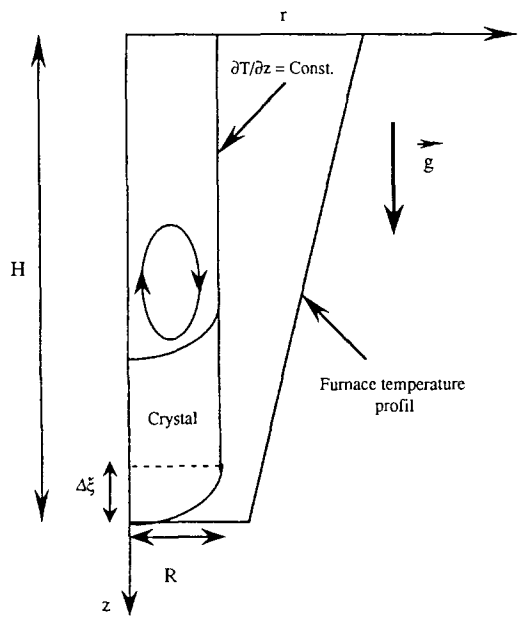

Fig. 1. Cavity configuration.

of momentum, heat and species) are made dimensionless using a viscous time $t^* = R^2/\nu$, a viscous velocity $\nu^* = \nu/R$, the crucible radius R, ∇TR and C_0 as scale quantities for time, velocity, length, temperature and concentration, respectively. In these expressions, ν is the kinematic viscosity and ∇T is the constant temperature gradient imposed by the heating facility. The dimensionless temperature is defined as $\theta = (T - T_c)/\nabla TR$, where T_c is the temperature of the interface. The domain containing the melt which varies during the solidification process is transformed into a fixed one using the following transformation: $z^* = z/S(r,t)$ and $r^* = r$, where $S(r,t)$ is the dimensionless length of the liquid area. According to these transformations and after the elimination of the asterisk *, the dimensionless governing equations in the liquid phase may be written in a vorticity-stream-function formulation as:

$$\frac{\partial\zeta}{\partial t} + u\frac{\partial\zeta}{\partial r} + (v - zv_f)\frac{1}{S}\frac{\partial\zeta}{\partial z} - \frac{\zeta u}{r} = \left[\frac{\partial^2\zeta}{\partial r^2} + \frac{1}{r}\frac{\partial\zeta}{\partial r} + \frac{1}{S^2}\frac{\partial^2\zeta}{\partial z^2} - \frac{\zeta}{r^2}\right] - \mathrm{Gr}\frac{1}{S}\frac{\partial\theta}{\partial z}, \tag{1}$$

$$\left[\frac{\partial^2\psi}{\partial r^2} - \frac{1}{r}\frac{\partial\psi}{\partial r} + \frac{1}{S^2}\frac{\partial^2\psi}{\partial z^2}\right] = r\zeta, \tag{2}$$

$$\frac{\partial\theta}{\partial t} + u\frac{\partial\theta}{\partial r} + (v - zv_f)\frac{1}{S}\frac{\partial\theta}{\partial z} = \frac{1}{\mathrm{Pr}}\left[\frac{\partial^2\theta}{\partial r^2} + \frac{1}{r} + \frac{\partial\theta}{\partial r} + \frac{1}{S^2}\frac{\partial^2\theta}{\partial z^2}\right], \tag{3}$$

$$\frac{\partial c}{\partial t} + u\frac{\partial c}{\partial r} + (v - zv_f)\frac{1}{S}\frac{\partial c}{\partial z} = \frac{1}{\mathrm{Sc}}\left[\frac{\partial^2 c}{\partial r^2} + \frac{1}{r}\frac{\partial c}{\partial r} + \frac{1}{S^2}\frac{\partial^2 c}{\partial z^2}\right], \tag{4}$$

where v_f is the dimensionless interface velocity ($v_f = RV_f/\nu$) and u and v, the velocity components defined as follows:

$$u = \frac{1}{r}\frac{\partial\psi}{\partial z}, \tag{5}$$

$$v = -\frac{1}{r}\frac{\partial\psi}{\partial r}. \tag{6}$$

The dimensionless parameters appearing in Eqs. (1)–(4) are the Grashof number $\mathrm{Gr} = g\beta\nabla TR^4/\nu^2$, the Prandtl number $\mathrm{Pr} = \nu/\kappa$ and the Schmidt number $\mathrm{Sc} = \nu/D$ (D is the dopant diffusivity). In the heat equation (3) the viscous dissipation is neglected.

2.2. Boundary conditions

At the horizontal rigid boundary, $z = 0$: $u = v = 0, \partial c/\partial z = 0$, and $\theta = S$.

At the growth interface, $z = 1$: $u = v = 0$, $\theta = 0$, and the rate of solute rejected into the melt is given by

$$\frac{1}{S}\frac{\partial c}{\partial z} = \mathrm{Pe}(1 - k)c - 2r\Delta\xi\frac{\partial c}{\partial r}, \tag{7}$$

where Pe stands for the Peclet number defined as $\mathrm{Pe} = RV_f/D = \mathrm{Sc}\, v_f$, and $\Delta\xi$ is the dimensionless interface deflection.

At the symmetry axis, $r = 0$: $u = 0, \partial c/\partial r = 0$, and $\partial T/\partial r = 0$.

At the crucible periphery boundary, $r = 1$: $u = v = 0, \partial c/\partial r = 0$, and for the temperature a linear pro-

file is maintained corresponding to the temperature gradient imposed by the heating facility.

At any moment, the fluid length is given by the relation: $h(r) = A - v_f t - \Delta\xi r^2$. This last relation shows that the growth interface is modelled as a paraboloid, and then is treated as an input such as the axial temperature gradient at the melt periphery.

The radial segregation is defined as follows:

$$\Delta c = \frac{cs_{max}(r,S) - cs_{min}(r,S)}{cs_{av}}, \qquad (8)$$

where cs_{av} is the average value of the concentration along the growth interface.

2.3. Numerical procedure

The governing Eqs. (1)–(4) are solved using an ADI (alternating direction implicit) technique with a finite-difference method involving forward differences for time derivatives and Hermitian relationships for spatial derivatives with a truncation error of $O(\Delta t^2, \Delta r^4, \Delta z^4)$ (see Hirsh [19] and Roux et al. [20]).

The mesh used to solve the problem (1)–(4) is generated by the Thompson technique [21]. We use a 25×101 grid which proved to give sufficiently accurate results for such studies (Kaddeche et al. [13,22]). Vertically (in the z direction), the nodes are constricted by the side walls and especially by the growth interface while in the horizontal direction the grid is symmetrical with the nodes crowded near the vertical side walls.

3. Validation of the numerical model

Our radial segregation results can be compared to the predictions of Coriell and Sekerka [9] who proposed an analytical solution valid for purely diffusive transport (Gr = 0) and low interface deflection. Our simulations indicate that Δc is a linear function of $\Delta\xi$, as shown in Fig. 2 for Pe = 0.1 and $k = 0.087$. At low $\Delta\xi$ the agreement with Coriell's results is excellent, but the discrepancy increases with increasing $\Delta\xi$. This was to be expected, since Coriell's solution does not hold at high curvatures. Other simulations performed with varying Pe numbers indicate that the numerical results are represented by the equation

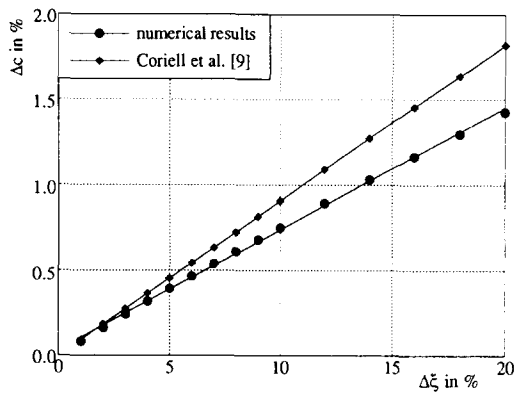

Fig. 2. Variation of the radial segregation Δc for the pure diffusive state.

$$\Delta c = 0.8\,\mathrm{Pe}(1-k)\Delta\xi \qquad (9)$$

for purely diffusive solute transport. Conversely, Coriell's results can be written as $\Delta c = (8/\pi^2)\mathrm{Pe}(1-k)\Delta\xi S(\mathrm{Pe},k)$, where $S(\mathrm{Pe},k)$ is a series depending on k and Pe and which is approximately equal to unity ($S(\mathrm{Pe},k) \sim 1$). Noticing that $8/\pi^2 \approx 0.81$, one can understand that the numerical and the analytical results are in good agreement.

Our simulations were also matched with Motakef's numerical results [8] in the vertical gradient freeze configuration. There, buoyancy-driven convection in the molten phase is generated by the radial temperature gradients due to the non-planarity of the solid–liquid interface. These gradients drive a convective cell constricted near the growth interface. The structure and the intensity of this cell is practically unchanged during the solidification process because of its position in the liquid phase (the size of the convective cell is less than the height of the liquid area) and because the temperature field remains almost constant for the low Prandtl number systems. The flow intensity is investigated over a wide range of the Grashof numbers ($\mathrm{Gr} \leq 5 \times 10^5$). As shown in Fig. 3, the flow intensity, the radial and the vertical velocity components scale linearly at first with the Grashof number. Nevertheless, for sufficiently high Grashof numbers, these quantities depart from the straight line, indicating that the inertial terms begin to be significant. In the limit of highly convective

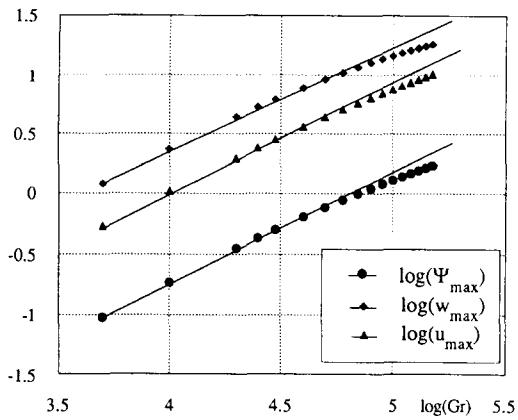

Fig. 3. Variation of Ψ_{max}, u_{max} and v_{max} as a function of Gr.

systems, the behaviour of Ψ_{max}, u_{max} and v_{max} is expected to be in $Gr^{1/2}$. The flow intensity is also seen to vary linearly with the solid–liquid interface deflection $\Delta\xi$, and our results show a quantitative agreement with those of Motakef [8]. These investigations lead to the fact that the effective driving parameter is $Gr_{eff} = \Delta\xi\ Gr$, as demonstrated by Motakef [8].

Finally, the predictions of our simulations were compared to the experimental results of Rouzaud et al. [18], who grew Ge:Ga alloys in a vertical gradient freeze furnace. Two pulling velocities $V_f = 8 \times 10^{-7}$ and 8×10^{-6} ms^{-1} were used, corresponding to Peclet numbers of 0.15 and 1.5, respectively. The other relevant parameters are $\Delta\xi = 6\%$, Gr = 46 500 and Sc = 7 [18]. The results presented in Table 1 in terms of both the convecto-diffusive parameter Δ (see Section 4) and radial segregation Δc show that our numerical simulations are overall in good agreement with the experimental data, except for the value of the convecto-diffusive parameter Δ corresponding to Pe = 1.5 (see Table 1).

Nevertheless, a private communication with Rouzaud [23] indicates that for the Pe = 1.5 experiment, the value of the interface deflection varies during the growth process between 3% and 6%. Consequently, we conducted further numerical simulations by taking into account this experimental observation. The results indicate that the value of the radial segregation is unchanged and that the new value of the convecto-diffusive parameter is equal to 0.65. This result is in excellent agreement with the experimental value of Δ ($\Delta_{exp} = 0.63$).

Table 1
Comparison of numerical and experimental results [18]

Pe	Δ_{num}	Δ_{exp}	Δc_{num}	Δc_{exp}
0.15	9×10^{-2}	9.5×10^{-2}	2.7%	2%
1.5	0.4	0.63	27%	25%

4. Longitudinal segregation

The analysis of axial segregation data is often done with reference to the pioneering work of Burton, Prim and Schlichter [24]. Assuming that whatever the convecto-diffusive state of the melt, a quasi steady state could be reached, these authors showed that the famous Scheil formula could be adapted using an effective partition ratio k_{eff} (see Ref. [14] for a detailed discussion of the question). Their work was later refined by Favier [25] who included the treatment of the initial transient in the segregation analysis.

It should be said that the physical basis of the stagnant film model used in these papers is rather shaky, a more correct approach relying on the concept of the solutal boundary layer, defined as the region in the vicinity of the interface where all significant concentration variations take place [14]. In practice however, the predictions of both models are in good agreement [26].

For the study of axial segregation, the numerically computed composition profiles in the solid are averaged normally to the growth direction and fitted using Favier's analysis [25]. The outcome of the procedure is the convecto-diffusive parameter Δ, that can be related to the effective partition k_{eff} via

$$k_{eff} = \frac{k}{1-(1-k)\Delta} \text{ with } \Delta = \frac{\delta V_f}{D}, \qquad (10)$$

where δ is the dimensional solutal boundary layer thickness. For diffusion controlled solute transfer conditions, δ is equal to D/V_f. It can thus be seen that Δ scales between 0 (total mixing) and 1 (diffusive transport). The effective partition coefficient is often used in practice, but for modelling purposes, the convecto-diffusive parameter is easier to handle and our results will be presented in terms of Δ.

At low convective levels, the laterally averaged axial composition data can be fitted using diffusive like profiles ($\Delta = 1$); the difference between purely diffusive and quasi-diffusive conditions can only be done when one considers radial segregation as will be done in Section 5. Briefly speaking, when solute transport is purely diffusive Δc is governed by the interface curvature; on the other hand, quasi-diffusive transport conditions may be characterized by the fact that Δc is governed by the interaction of fluid flow and established axial composition gradients. In this section, special emphasis will be laid on the well-mixed regimes where convection is strong and leads to significant deviations from diffusive axial segregation profiles.

In all the numerical simulations, the interface deflection is taken to be $\Delta\xi = 6\%$ and $\mathrm{Pr} = 0.007$. In practice, heat transport being mainly diffusive, thermal convection has no effect on interface curvature in vertical Bridgman growth of low Prandtl number alloys. The relevant parameters of the problem are: Gr, Sc, Pe and k. This set of parameters can be divided into two groups, the first is composed by Pe and k appearing in the solute interface boundary condition, and the second contains the Gr and the Sc which appear in the momentum and species conservation equations.

Shown in Fig. 4 is the variation of Δ as a function of the Schmidt number Sc, the Peclet number $\mathrm{Pe} = RV_f/D$ being equal to 0.6, the other relevant values being $\mathrm{Gr} = 15 \times 10^4$ and $k = 0.087$. In such a situation, where convection dominates mass transport ($\Delta \ll 1$), it appears clearly that Δ scales with $\mathrm{Sc}^{-1/3}$.

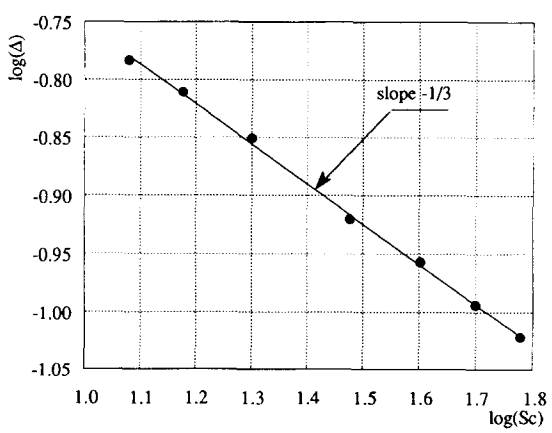

Fig. 4. Variation of the convecto-diffusive parameter Δ as a function of Sc.

Simulations carried out with varying Peclet numbers indicate that Δ is proportional to Pe in the low Pe range, and Δ thus scales with $\mathrm{PeSc}^{-1/3}$ in the convective regime limit. Such a behaviour can be understood from simple order of magnitude analysis arguments. Indeed, let us consider the characteristic equation for the solutal boundary layer,

$$\frac{D}{\delta} = V_f - W(\delta), \tag{11}$$

where $W(\delta)$ denotes averaged vertical fluid velocity toward interface, taken at solutal boundary layer scale [12,14]. Continuity arguments indicate that $W(\delta)$ varies with $(\delta/R)^2$, close to the growth front. Setting $W(\delta) = -\alpha(v/R)(\delta/R)^2$, we get for the convective regime limit ($-W(\delta) \gg V_f$):

$$\frac{\delta}{R} \sim (\alpha\,\mathrm{Sc})^{-1/3} \text{ and } \Delta \sim \mathrm{Pe}(\alpha\,\mathrm{Sc})^{-1/3}. \tag{12}$$

When the Grashof number is smaller than circa 5×10^3, the factor α is proportional to Gr and one falls back on $\mathrm{Pe}\,(\mathrm{Gr\,Sc})^{-1/3}$ scaling law identified in the horizontal Bridgman problem [12–14]. In practice, assuming the departures from proportionality to be limited, our numerical results in the convective transport regime can be written as

$$\Delta = 33.7\,\mathrm{Pe}(\mathrm{Gr}\cdot\mathrm{Sc})^{-1/3} \tag{13a}$$

or equivalently

$$\Delta = 13.2\,\mathrm{Pe}(\mathrm{Gr_{eff}Sc})^{-1/3} \tag{13b}$$

if we want to use the physically relevant $\mathrm{Gr_{eff}} = \Delta\xi$ Gr. Strictly speaking, the well-mixed transport regime is defined by the condition $\Delta \ll 1$, with Δ given by Eq. (13). In practice, the condition $\Delta \leq 0.2$ can be used to characterize the convection dominated transport mode.

5. Radial segregation

Our aim through the following investigation is to estimate quantitatively the rate of radial segregation, especially its dependence on the various system parameters for the different convection regimes (diffu-

sive, quasi-diffusive and well-mixed regimes). Due to the essentially transient nature of the solidification process, radial segregation changes with position along the crystal. However, the normalized composition variations, as defined in Eq. (8), are seen to reach a plateau after an initial transient (see Fig. 5). In the following, the phrase "radial segregation" will refer to the level of the plateau.

First, we investigated the influence of the segregation coefficient and the Peclet number on the rate of radial segregation defined above. Holding all the other parameters constant, we conducted a set of calculations with different values of the segregation coefficient, $k = 0.1, 0.2, \ldots, 0.9$. The results indicate that the rate of radial segregation Δc is a linear function of $1 - k$ for all the convective regimes. Similar calculations are conducted for different Peclet numbers; Δc is seen to vary linearly with the Peclet number for Pe between 0.014 and 7. Combining these first results, we can conclude that the rate of radial segregation Δc, in the range of investigated k and Pe, is a linear function of $\mathrm{Pe}(1 - k)$.

We then focused our investigations on the interaction between convection and segregation by varying the Grashof number for $k = 0.087$, $\mathrm{Sc} = 10$ and $\mathrm{Pe} = 0.2$. As shown in Fig. 6, the curve giving the variation of Δc with Gr could be divided in three parts depending on the mixing level of the melt. The first part ($\mathrm{Gr} \leq 10$) corresponds to the diffusive state during which Δc is almost constant and equals to 0.88%. This lateral segregation is due to the interface deflection. During the second part ($200 \leq \mathrm{Gr} \leq 3000$)

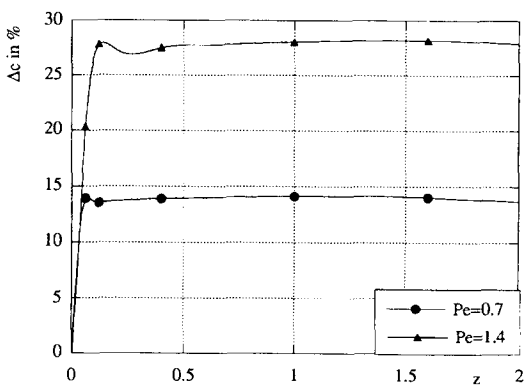

Fig. 5. Variation of the radial segregation Δc for $\mathrm{Gr} = 5000$, $k = 0.087$, $\Delta\xi = 6\%$ and different values of Pe.

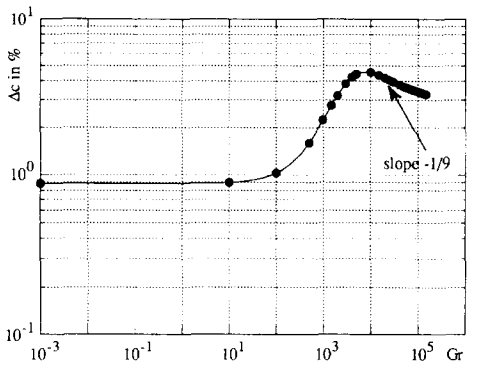

Fig. 6. Variation of the radial segregation Δc as a function of Gr.

corresponding to the quasi-diffusive state, the rate of radial segregation Δc is a linear function of Gr. The maximum radial segregation rate is obtained for $5000 \leq \mathrm{Gr} \leq 10\,000$ and corresponds to the critical point where the interference between convection and segregation produces the most important radial segregation for the considered system. Above this point ($\mathrm{Gr} \geq 15\,000$), begins the third part of the curve which corresponds to the well-mixed state. In this part, the rate of radial segregation Δc follows an asymptotic $\mathrm{Gr}^{-1/9}$ power law in Gr.

Finally, we considered the influence of the Schmidt number on Δc in the quasi-diffusive and the well-mixed state, using again $k = 0.087$ and $\mathrm{Pe} = 0.2$. For the quasi-diffusive regime, numerical calculations indicate that Δc is proportional to the Schmidt number. On the other hand, when convection dominates mass transport Δc follows a $\mathrm{Sc}^{-2/9}$ power law. Combining all the results, one can write

$$\Delta c = 0.64 \times 10^{-5}(1 - k)\,\mathrm{Pe}\,\mathrm{Gr} \cdot \mathrm{Sc}, \qquad (14a)$$

$$\Delta c = 1.1(1 - k)\,\mathrm{Pe}\,\mathrm{Gr}^{-1/9}\mathrm{Sc}^{-2/9} \qquad (14b)$$

for the quasi-diffusive and well-mixed state, respectively.

An interesting parallel can again be drawn with the horizontal Bridgman configuration studied previously [15,16]. In the quasi-diffusive regime, Δc was seen to scale linearly with $\mathrm{Pe}(1 - k)\mathrm{Gr}\,\mathrm{Sc}$ at low Pe numbers [16]. Such a behaviour was explained from order of magnitude arguments; indeed, it can be said that radial segregation is a result of an interaction of the flow (intensity scaling with $\mathrm{Gr}\,\mathrm{Sc}$) with an existing concentration gradient ahead of the interface

(proportional to Pe(1 − k)). Such an explanation can also be proposed for the vertical Bridgman configuration, provided that the convection related Δc exceeds the curvature related Δc, which of course depends on the interface deflection.

In practice, one may expect that the linear Pe(1 − k)Gr Sc regime will not be observed when the curvature of the growth front is too high. Furthermore, the proportionality relation between Δc and the Peclet number can not hold at high Pe, since radial segregation can not increase indefinitely. From the order of magnitude analysis, a Pe^{-3} scaling law was identified in the large Pe limit for the horizontal Bridgman configuration; such a behaviour was not observed here, but it should be kept in mind that our Peclet numbers remained limited (Pe < 7).

The situation is more complex in the well-mixed state, where a Pe $(1-k)$ $(Gr\,Sc)^{-2/9}$ dependence was identified from numerical and scaling analysis arguments in the horizontal problem, even though some of the arguments proposed in Ref. [15] are still of interest here. Indeed, when convection dominates solute transport, the interface composition may be considered as quasi-uniform, and all concentration variations are then expected to scale with $Pe(1-k)$. However, the discussion that led to the $(Gr\,Sc)^{-2/9}$ variation in the horizontal Bridgman problem could not be adapted for the vertical case and the $Sc^{-2/9}$ behaviour observed here (see Eq. (14b)) should be considered as fortuitous. In our previous study [15], the fluid velocity was constrained to remain proportional to the Grashof number. Quite generally, it can be demonstrated that in such a case the convective mass transport intensity in the melt scales with the product of the Grashof and Schmidt numbers. The distinct power law exponents of Gr and Sc in Eq. (14b) thus indicate that there was a departure from the purely laminar hydrodynamic regime.

6. Concluding remarks

Our purpose in this paper was to investigate the interference between natural convection and macrosegregation in the vertical Bridgman growth configuration. A detailed numerical modelling allowed us to cover a wide range of solute transport conditions, ranging from the purely diffusive to the well-mixed state. The numerical results are presented in the form of scaling laws relating non-dimensional parameters that can be easily a priori derived from experimental variables. We also show that these scaling laws can often be understood with the help of simple order of magnitude arguments adapted from the study of the horizontal Bridgman configuration.

The only open question concerns the segregation dependence on the Grashof number in the well-mixed regime. As the fluid velocity ceases to be proportional to Gr, it becomes very difficult to measure the convective intensity in the mass transport problem. A mass transport Peclet number Pe_m as defined by Motakef [8] is an interesting possibility, but the drawback is that Pe_m can not be derived a priori from the experimental parameters. Besides, Motakef's averaging procedure (see Eq. (17) in Ref. [8]) should probably be adapted for the case where the solutal boundary layer thickness is strongly reduced, i.e., for the well-mixed regimes considered in our present work.

The situation is specially intricate when dealing with the radial segregation problem, where our $Gr^{-1/9}$ power law should be compared to other literature results. Adornato and Brown [5] proposed a $Gr^{-1/7}$ behaviour, whereas a recent paper by Tanveer [27] identified a $Gr^{-1/6}$ dependence. However, it should be kept in mind that both the $Gr^{-1/7}$ and $Gr^{-1/6}$ power laws come from the modelling of the three zone furnaces, which may account for the discrepancy with our results. Anyway, more work on this point would certainly be necessary for a definite conclusion to be drawn.

With this restriction in mind, let us proceed to see how a given experiment can be characterized from our modelling. The first thing to do is to identify the relevant non-dimensional parameters Gr, Sc, Pe, $\Delta\xi$ and k from thermophysical data, process variables and a measurement of the interface deflection. Then, Eq. (13) can be used to discriminate between the diffusion dominated and convection dominated solute transport modes.

If mass transport is principally diffusive, a distinction should yet be made between the curvature related radial segregation, as given by Eq. (9), and the convection related radial segregation, as given by Eq. (14a). In the well-mixed regime, we think that Eq. (14b) can safely be used in practice to get a first

estimate of Δc, even though, as discussed previously, the situation is far from being clear in terms of Gr dependence.

To conclude with, we would like to stress again the originality of our approach with respect to previous works in the field. Instead of a detailed modelling of a given growth experiment, we are more interested in using the numerical simulations to capture the physics of the transport phenomena and to offer a variety of scaling laws that can be easily used by the practician. In the future, we shall try to adapt this approach to related problems, e.g., the effect of thermosolutal convection and aspect ratio, or a coupling with the phase diagram.

Acknowledgements

The authors are indebted to Dr A. Rouzaud from the CEN Grenoble for fruitful discussions. The present work has been conducted within the frame of the GRAMME agreement between the CNES and the CEA, the CNES microgravity program and the CNRS-PIRMAT solidification program. Computations were carried out on the C98 computer, with the support of the "Institut du développement et des ressources en informatique scientifique" (IDRIS).

References

[1] W.A. Gault, E.M. Monberg and J.E. Clemans, J. Crystal Growth 74 (1986) 491.
[2] F. Allegretti, B. Borgia, R. Riva, F. De Notasristefani and S. Pizzini, J. Crystal Growth 94 (1989) 373.
[3] Y. Huang, W.J. Debnam and A.L. Fripp, J. Crystal Growth 104 (1990) 315.
[4] C.J. Chang and R.A. Brown, J. Crystal Growth 63 (1983) 343.
[5] P.M. Adornato and R.A. Brown, J. Crystal Growth 80 (1987) 155.
[6] D.H. Kim and R.A. Brown, J. Crystal Growth 109 (1991) 66.
[7] D.H. Kim and R.A. Brown, J. Crystal Growth 114 (1991) 411.
[8] S. Motakef, J. Crystal Growth 102 (1990) 197.
[9] S.R. Coriell and R.F. Sekerka, J. Crystal Growth 46 (1979) 479.
[10] S.R. Coriell, R.F. Boivert, R.G. Rehm and R.F. Sekerka, J. Crystal Growth 54 (1981) 167.
[11] S.A. Korpela, A. Chait and D.H. Matthiessen, J. Crystal Growth 137 (1994) 623.
[12] J.P. Garandet, T. Duffar and J.J. Favier, J. Crystal Growth 106 (1990) 437.
[13] S. Kaddeche, H. Ben Hadid and D. Henry, J. Crystal Growth 135 (1994) 341.
[14] J.P. Garandet, J.J. Favier and D. Camel, in: Handbook of Crystal Growth 2, Ed. D.T.J. Hurle (North-Holland, Amsterdam, 1994).
[15] J.P. Garandet, J. Crystal Growth 114 (1991) 593.
[16] J.P. Garandet, J. Crystal Growth 125 (1992) 112.
[17] J.P. Garandet, J. Crystal Growth 131 (1993) 431.
[18] A. Rouzaud, D. Camel and J.J. Favier, J. Crystal Growth 73 (1985) 149.
[19] R. Hirsh, J. Comput. Phys. 19 (1975) 90.
[20] B. Roux, P. Bontoux, T.P. Loc and O. Daube, in: Lecture Notes in Mathematics, Vol. 771, Ed. R. Rautmann (Springer, Berlin, 1980) pp. 450–468.
[21] J.F. Thompson, Z. Vawarsi and C.W. Mastin, Numerical Grid Generation (Elsevier, Amsterdam, 1985).
[22] S. Kaddeche, H. Ben Hadid and D. Henry, J. Crystal Growth 141 (1994) 279.
[23] A. Rouzaud, personal communication.
[24] J.A. Burton, R.C. Prim and W.P. Schlichter, J. Chem. Phys. 21 (1953) 1987.
[25] J.J. Favier, Acta Met. 29 (1981) 197.
[26] J.P. Garandet, to appear in Current Topics in Crystal Growth Research, Research Trends 1995.
[27] S. Tanveer, Phys. Fluids 6 (1994) 2270.